Detectors in positron emission tomography

Artem Zatcepin [a,b], **Sibylle I. Ziegler** [a,*]

[a] Department of Nuclear Medicine, University Hospital, LMU Munich, Munich, Germany
[b] German Center for Neurodegenerative Diseases (DZNE), Munich, Germany

Received 11 July 2022; accepted 25 August 2022

Abstract

Positron emission tomography is a highly sensitive molecular imaging modality, based on the coincident detection of annihilation photons after positron decay. The most used detector is based on dense, fast, and luminous scintillators read out by light sensors. This review covers the various detector concepts for clinical and preclinical systems.

Keywords: Positron emission tomography (PET); PET detectors; Avalanche photodiode; Silicon photomultiplier; Photomultiplier tubes

Requirements for PET detectors

After emission during positron decay, positrons lose energy in the surrounding tissue and finally annihilate with an electron. Positron imaging relies on the fact that in the annihilation process two photons with 511 keV energy each are simultaneously emitted back-to-back. By detecting these photons within a very short time window, a line-of-response (LOR) can be determined without geometrical collimation (as it is needed in gamma camera-based single photon emission tomography imaging). This coincidence mode of acquisition is the reason for the excellent sensitivity of positron emission tomography (PET).

Several requirements for the detection system follow from this basic principle:

- Detection efficiency for photons with 511 keV needs to be high since the coincidence efficiency is the product of efficiencies of two channels.
- For effective reduction of scattered radiation in the measured signal, the detectors need to provide accurate information on the energy deposited in a detector element.
- The detectors need to be fast in order to operate with short coincidence windows, reducing the number of random coincidences and potentially providing time-of-flight information.
- The detection elements need to be small since their size determine the achievable spatial resolution.

Scintillation detectors still remain the type of detectors that fulfill these requirements best. They are based on a piece of scintillator read out by a light sensor. Since the first PET designs, research in scintillation crystals and light sensors has tremendously improved PET detectors as well as overall system performance.

In this brief review, we describe most important developments in PET detector technology leading to the current state-of-the-art.

Scintillation crystals

The requirements listed above translate into properties of scintillation crystals [1]: Dense materials with high atomic number offer high interaction probability and high photofraction. Energy resolution is strongly influenced by photon statis-

* Corresponding author: Sibylle I. Ziegler, Department of Nuclear Medicine, University Hospital LMU Munich, Marchioninistrasse 15, D-81377 München, Germany.
E-mail: Sibylle.ziegler@med.uni-muenchen.de (S. I. Ziegler).

https://doi.org/10.1016/j.zemedi.2022.08.004
www.elsevier.com/locate/zemedi

Table 1
Examples of scintillation materials used in PET detectors (data from [11,12]). Z_{eff} is the effective atomic number.

Material	Density (g/cm^3)	Z_{eff}	Light output (photons/keV)	Decay time (ns)	Hygroscopic
NaI:Tl	3.67	51	41	230	yes
BGO	7.1	75	9	300	no
L(Y)SO:Ce	7.1-7.4	65-66	26-34	38-44	no
BaF_2	4.9	54	1.3-1.4	0.8	no
CsF	4.6	52	1.9-2.0	3	yes
$LaBr_3$:Ce	5.1	45	64-76	16	yes

tics; thus, luminous scintillators are preferred. In addition, high light yield facilitates readout schemes beyond one-to-one coupling of scintillation crystal and light sensor. Fast emission of the scintillation light results in precise time stamping of events. The scintillation wavelength needs to be in the range of optimal detection of the light sensor with little self-absorption inside the crystal element. Furthermore, matching index of refraction ensures little light loss between crystal and light sensor. Rugged materials are advantageous as they can be cut in small individual pieces without cleavage. Some scintillation materials are hygroscopic, thus special care must be taken in their encapsulation.

The first positron imaging devices were based on Thallium-doped sodium-iodine (NaI(Tl)) crystals, well known from Anger gamma cameras. Each crystal was read out by a photomultiplier tube, limiting the smallest possible size of individual detection elements. In the first device which was used for in vivo scanning, pairs of NaI(Tl) detectors ($3 \times 3 \times 4$ cm^3) were operated in coincidence and translated laterally, yielding a 2D projection of positron emitter density in the brain [2]. NaI (Tl) is a bright scintillator, but with density of 3.67 g/cm^3 and effective atomic number of only 51, its detection efficiency for 511 keV photons is low. Therefore, once the high-Z scintillator bismuth germanate (BGO) became available in the early 1970s [3], it quickly came into the focus as an alternative PET scintillator [4] and was the scintillator of choice for many years in PET instrumentation.

About 20 years later, the development of fast, luminous crystals resulted in a new generation of PET scanners. In the early 1990s, the growth of cerium-doped lutetium oxyorthosilicate (LSO:Ce) was established [5]. Later, LYSO:Ce was introduced, which requires a lower melting temperature in the crystal growing process [6]. Both, LSO and LYSO, have similar density as BGO, a little lower atomic number, but are much brighter and faster than BGO. Therefore, much better timing and energy resolution could be achieved without reducing the detection efficiency too much.

Scintillation materials with even faster decay times are cesium fluoride (CsF) or barium fluoride (BaF_2). They have been used already in the 1980s for the first time-of-flight PET scanners [7–9] with coincidence timing resolution between 500 and 750 ps. Both materials have low detection efficiency and low light yield, resulting in lower system performance compared to BGO-based scanners. $LaBr_3$:Ce scintillation material has also a short decay time, but also an excellent light yield and energy resolution. Unfortunately, its density and atomic number are similar as in CsF and BaF_2, thus detection efficiency is limited. Nevertheless, a LaBr3:Ce based tomograph was built showing the impact of timing and energy resolution on image quality [10].

Some characteristics of scintillators used for PET are summarized in Table 1.

Light sensors

The weak scintillation light needs to be converted in an electrical signal, which can be analyzed for time of arrival and total amount of light. Thus, the light sensors used in a detection system must be selected according to the properties of the scintillation light. Most importantly, detection efficiency for the scintillation light (e.g. 420 nm in LSO:Ce) and charge amplification need to be high, while signal rise time should be as short as possible. In addition, linear response with respect to the amount of emitted scintillation light is assumed. The standard light sensor in PET detectors has been the photomultiplier tube. Although silicon-based light sensors have been used since many years as well, their implementation in large PET systems with excellent performance is still very recent.

Photomultiplier tubes

Most PET detectors produced up to now have been based on photomultiplier tubes (PMTs). A PMT is a vacuum glass tube that contains a photocathode, a series of electrodes with increasing voltage called dynodes, and an anode. The incident photons that come through the glass window collide with the photocathode producing photoelectrons (efficiency at 420 nm is approx. 30%). These primary photoelectrons travel in the direction of the first dynode accelerated by the voltage difference between the photocathode and the first dynode. As they hit the dynode, secondary electrons are generated. This process is then repeated at each progressive dyn-

ode, resulting in signal amplification of up to 10^6 depending on the PMT design [13]. Thanks to the vacuum environment of PMTs, their advantage over solid-state sensors is a relatively low dark count rate (in the order of tens of counts per second [14]), which is the number of output pulses originating from electrons randomly emitted by the photocathode and the dynodes per unit time. In addition, signal rise time is typically very short.

The development of square multi-anode, position-sensitive PMTs (PSPMT, flat panel PMT) [15] with e.g. 64 readout channels covering an area of approx. 5×5 cm^2 opened up a new era of high-resolution detectors [16]. Owing to their compact size and minimum housing, these light sensors were key for the advancement of small animal PET instrumentation and organ-specific PET systems.

Avalanche Photodiode

Once solid state photon sensors with appropriate characteristics became available [17], avalanche photodiodes (APD) were investigated as light sensors for PET detectors. In contrast to a regular p-i-n photodiode, where an incident photon generates only one electron-hole pair, an APD provides internal signal amplification, which is essential for PET application. In an APD, an electron produced by the incident photon gets accelerated by a large reverse voltage and then collides with the lattice producing a new electron-hole pair. This process can then be repeated by the same electron as well as by the newly generated electron, creating an avalanche effect and resulting in significant signal amplification [18]. However, the typical internal gain achieved by APDs used in PET is around 100 [19], which is significantly lower compared to PMTs. Moreover, the timing resolution of APDs is in the range of several ns, thus inferior to the one exhibited by PMTs [20]. In PET, APDs are operated in proportional mode, i.e., the reverse voltage is set in a way that the generated signal is proportional to the amount of incident scintillation light [21]. Compared to PMTs, APDs have significantly higher quantum efficiency (80% versus 30%) and can be employed in high magnetic fields [22], which enabled their use for combined PET/MR imaging [23–25]. The first commercial simultaneous PET/MR system for clinical use is based on APDs [26].

Furthermore, they can be produced as compact arrays of individual small APDs (Fig. 1 [19]).

Silicon Photomultiplier

Silicon photomultipliers (SiPMs) aim at combining the benefits of PMTs and APDs. SiPMs produce gains equal or greater to those of PMTs, while requiring only moderate reverse voltage (below 100 V) [27]. Similarly to APDs, SiPMs are not susceptible to magnetic fields [28] and can be employed in PET/MR imaging [29,30]. Compared to APDs, SiPMs exhibit superior timing resolution below 1 ns [31] which makes them suitable for time-of-flight PET [32]. A SiPM consists of an array of parallelly-connected APDs functioning in Geiger mode, i.e. operating above the breakdown voltage. This voltage creates an electric field across the depletion region that is large enough to make the impact ionization process self-sustaining [17]. Such Geiger-mode APDs generate a large output signal even for a single incident photon. Therefore, they are also known as single-photon APDs (SPADs). Thus, the number of incident photons cannot be estimated by an individual SPAD. A SiPM overcomes this issue by using an array of very small SPADs (Fig. 2). By adding the signals of all SPADs in the array, the SiPM signal is proportional to the number of photons reaching the surface of the SiPM if the number of available SPADs is larger than the number of entering photons. For bright scintillators this may not be the case, and non-linear response needs to be corrected for.

Just like PMTs, the analog output signal of SiPMs is proportional to the amount of detected scintillation light and needs to be read out and digitized with appropriate electronics for energy and timing information. Digital SiPMs, on the other hand, integrate counting electronics on the SiPM wafer

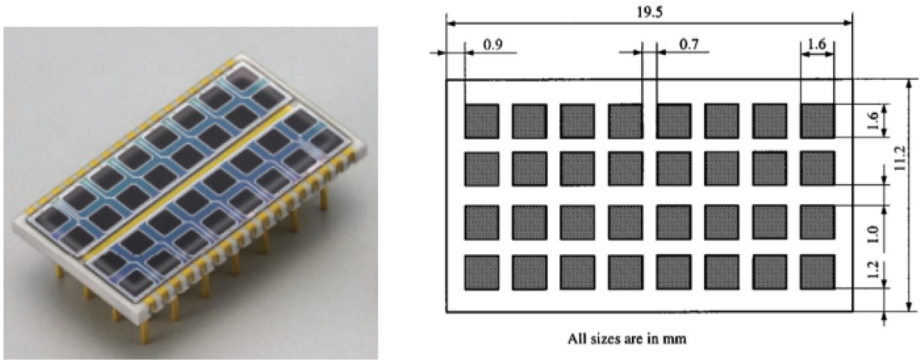

Figure 1. Example of an array of small APDs, each with a sensitive area of 1.6×1.6 mm^2. (Hamamatsu Photonics KK, Japan) [19].

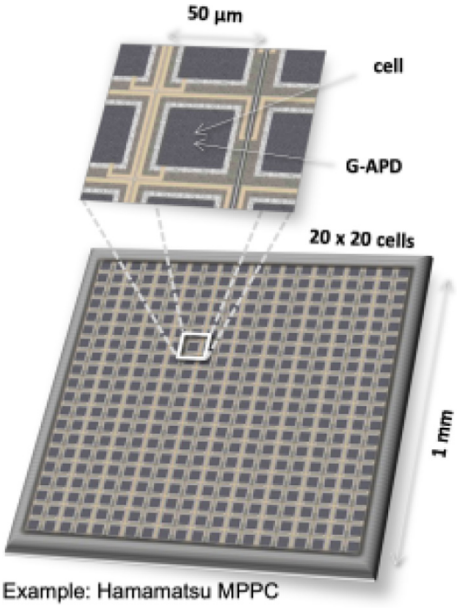

Figure 2. Example of an SiPM with $1 \times 1\text{mm}^2$ sensitive area with 20×20 individual APDs operated in Geiger mode (G-APD). Each cell outputs a standard pulse when hit by a photon. The number of "firing" cells is proportional to the number of detected scintillation photons [33].

(reducing the sensitive area somewhat), thus the output is the number of fired SPADs, eliminating the need of analog readout electronics [34]. These digital SiPMs are the light sensor used in a clinical PET/CT device [35] and have recently been used in the development of a large axial field-of-view tomograph [36].

Detectors

Several schemes of combining scintillation crystals with light sensors have been developed since the first prototype PET scanners (Fig. 3, [37]).

One-to-one coupled detectors

First PET detectors comprised a single scintillation crystal coupled to a single PMT. The intrinsic spatial resolution of such a system is defined by the size of the crystal cross-section. Therefore, to improve the resolution, one would need to reduce the crystal size and, to maintain the same sensitivity, to increase the total number of detectors. With PMTs being bulky, the size reduction is limited, while using a greater number of detectors is associated with an increased system cost. A solution to this problem was the block detector [38]. However, some modern preclinical systems use one-to-one coupling [29,39,40]. In such scanners, the size reduction is achieved by using SiPMs instead of PMTs.

Block detectors

A block detector was the next step in PET detector development to achieve modules with closely packed, small crystal elements [38]. A typical block detector consists of a cubic scintillation crystal optically coupled to a photodetector array (originally PMTs). The scintillator has perpendicular cuts starting from the frontal surface (Fig. 4). The cuts are filled with a reflective material. The depth of the cuts increases in the direction of the corners, starting from approximately half of the crystal depth up to almost full depth, to create a linear light distribution among the PMTs. The position of a scintillation event is estimated by Anger logic [41], with events being clustered at specific points corresponding to the individual elements of the scintillator. Using a lookup table derived from uniform irradiation of the scintillator, one can assign each event to a certain scintillator element [38].

A typical configuration consists of 8×8 individual crystal elements read out by only four PMTs (Fig. 4). Such a design allows to significantly reduce the number of readout channels and system cost compared to the one-to-one coupling.

Continuous detectors

Similar to block detectors, continuous detectors consist of a large scintillation crystal optically coupled to a photodetector array (PSPMT or APD/SiPM array), but the crystal does not have cuts in it. This approach aims at maximizing the sensitivity, as there are no individual elements with gaps

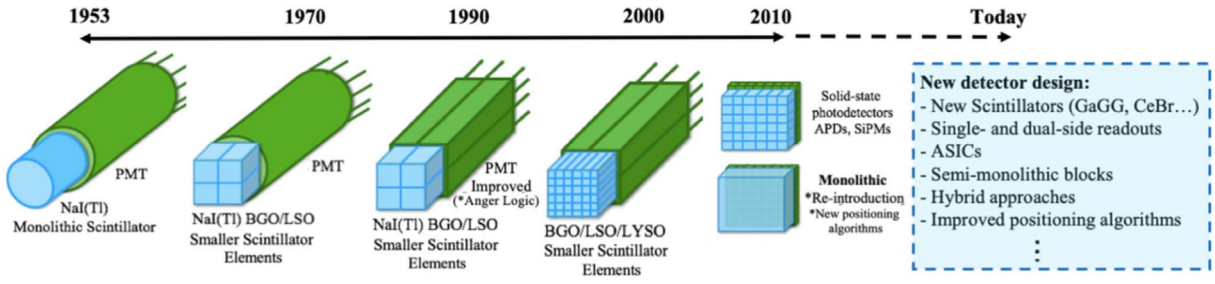

Figure 3. Development of PET detector design [37].

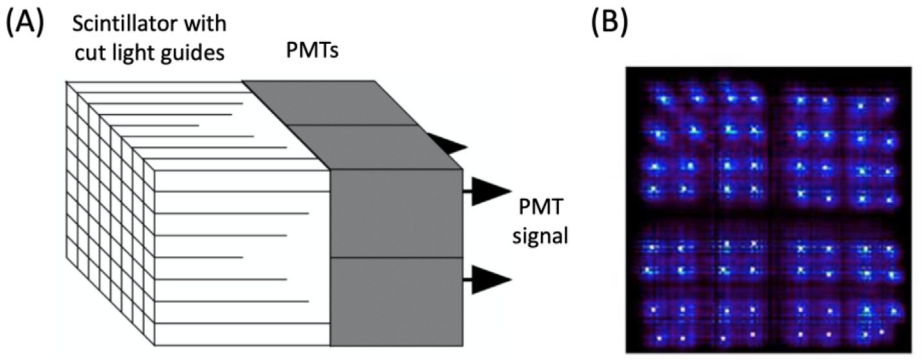

Figure 4. Principle of the block detector. (A) A matrix of 8 × 8 crystals is read out by 4 PMTs using Anger-type crystal identification. (B) Flood map of one block showing the position of the 64 crystal elements. Modified from [42,43].

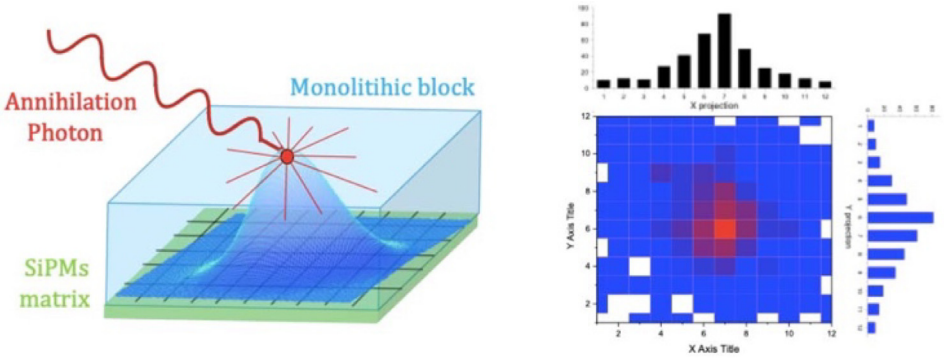

Figure 5. Light distribution from an annihilation photon within a monolithic scintillator (left) and the corresponding flood map profiles (right) [37].

in between [44,45,46], while further reducing the system cost owing to the reduced manufacturing costs. The estimation of the event position is achieved by analyzing the light distribution shape (Fig. 5). There are three types of positioning methods: analytical, statistical, and machine learning-based. The analytical methods operate with two- and three-dimensional light distribution models. The statistical methods include least square, chi square, nearest neighbors, and maximum likelihood. Some examples of machine learning-based methods are neural networks, gradient tree boosting, and support vector machines. More details can be found in a recent review article [37].

In modern continuous detectors it is possible to achieve a sub-millimeter spatial resolution [47–49], as monolithic crystals do not have individual elements limiting the resolution by their cross-section size.

One of the disadvantages of using continuous detectors is the need for a lengthy detector calibration when using statistical positioning algorithms, which usually requires complex algorithms and substantial computational power, followed by a hardware setup [50]. Additionally, the estimation of the position of Compton interaction in monolithic crystals is problematic [51]. Another challenge is the truncation of scintillation light close to the crystal edges. Several approaches were proposed to cope with this effect, including the use of optical absorber on the crystal edges [52], double-sided readout, allowing the light to pass into the adjacent monolithic crystals [53], the use of trapezoid crystals [54], edge readout [55].

Depth-of-interaction detectors

The need for depth-of-interaction (DOI) estimation arises when one aims at achieving high sensitivity while maintaining high spatial resolution, which is the case in preclinical PET scanners, where the size of the subject to be scanned and the amount of injected activity is much smaller compared to clinical systems [56]. A way to achieve high sensitivity is to use long and narrow scintillation crystals (Fig. 6). This, however, comes with a problem that if a source is located at a certain radial offset from the field-of-view center, the generated annihilation photons might pass the first crystal on their way without an interaction and then produce a scintillation deep within the adjacent crystal, as shown in

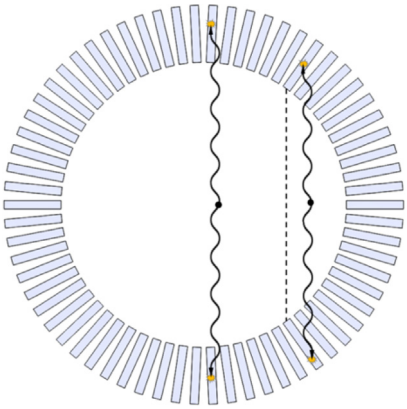

Figure 6. Detector parallax effect. The line-of-response on the right is mispositioned towards the field-of-view center (dashed line).

Fig. 6. If the interactions are assigned to a fixed location, e.g., the crystal center or entrance, which is the case in non-DOI-encoding systems, such lines-of-response will be mispositioned. This is called the parallax effect, which results in the degradation of the radial component of spatial resolution [57].

One way to estimate the DOI is to utilize monolithic scintillators and 3D localization algorithms based on the light distribution across the light sensor array. DOI resolution below 3 mm was achieved for 20 mm thick monolithic scintillators [52].

Alternatively, one can use two or more scintillation crystals with different decay times and pulse shapes coupled to each other with an optical grease along their axis. Such a design is also known as phoswich detector [58–60]. The DOI resolution of such a detector is roughly the height of the individual crystals composing the detector. However, it requires materials of sufficiently different light emission times and appropriate electronics. Some other approaches use multi-layer offset crystal designs [61–63] or multi-layer crystals with edge readout [64–66].

Another way to measure the DOI is to use double-sided readout without changing the scintillators themselves. In this design, the lateral sides are unpolished, so that the ratio of the scintillation light detected at the two ends of the crystals is proportional to the DOI [67]. This method yields high precision of DOI estimation. For instance, Abreu et al. [68] demonstrated 2 mm DOI resolution for their system. However, the double-sided readout largely increases both the cost and the complexity of the system. Pizzichemi et al. [69] proposed a single-sided readout-based method, where the crystal array is equipped with a light guide and a reflector on the side opposite to the SiPM readout. This setup allows detection of the light emitted in both directions using a single SiPM array. The average DOI resolution achieved by using this method was shown to be 3 mm for an 8×8 array of $1.53 \times 1.53 \times 15$ mm^3 Ce:LYSO crystals when using a machine learning-based positioning algorithm [70]. In another single-sided readout method, the crystals are coated with phosphor on their sides to make the pulse shape DOI-dependent. Berg et al. [71] were able to achieve a sub-2-mm DOI resolution with such a detector using maximum likelihood pulse shape discrimination.

Time-of-flight detectors

Time-of-flight (TOF)-PET is a technology aiming at limiting the region along the line-of-response within which the positron annihilation occurred [11]. TOF-PET estimates the position of the annihilation event by measuring the difference of the arrival times between the two annihilation photons in the opposing detectors (Fig. 7).

To enable TOF measurements, the PET detector needs to fulfill specific characteristics. The scintillation process should have instantaneous rise and decay times of the light pulse profile. While there is no ideal material (yet), L(Y)SO:Ce, BaF_2, CsF, and $LaBr_3$:Ce have been used in TOF-PET detectors. The photodetector should have high detection efficiency of the scintillation light, low noise, and instanta-

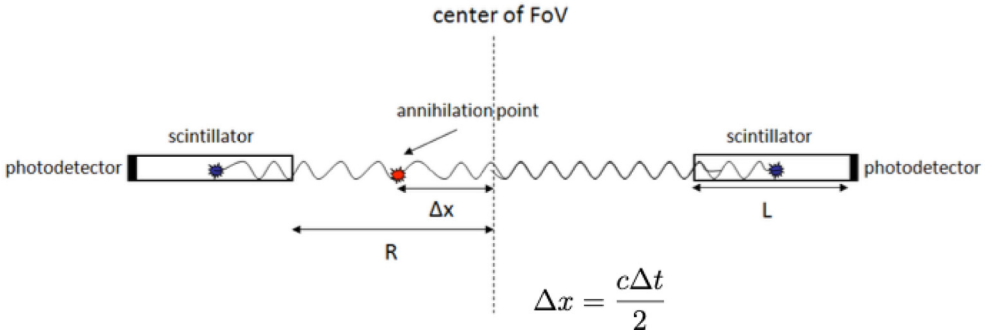

Figure 7. TOF-PET concept: By measuring the difference in arrival times the position of the annihilation event along the line-of-response can be determined (c: speed of light). Adapted from [32].

neous rise and decay time of the charge pulse profile as well as low charge transit time spread [32]. Both, PMTs and SiPMs are currently used for TOF-PET detectors. In combination with appropriate electronic readout, timing resolution of a few hundred ps can be achieved in clinical PET scanners [11].

Systems

Clinical PET devices have evolved from two detector elements measuring one coincidence line at a time to systems with 564,480 crystals simultaneously covering the whole human body, acquiring almost 10^{11} lines-of-response [72]. The idea of building a PET device that, because of its maximum solid angle coverage [73], could reach sensitivity ranges that would allow very low-activity examinations was taken to clinical use in the Explorer project [74]. Motivated by this success, there are several research activities and products delivering total-body PET or PET with large axial field of view of 1 to 2 m [75].

In addition to the very good scalability of SiPM-based detectors, total-body PET also benefits from the excellent time resolution value of 210 ps achieved in the new systems [76]. This corresponds to a spatial uncertainty of the emission point along the line-of-response of 3.2 cm. While this does not directly improve the spatial resolution in the tomograph, the time-of-flight information in the image reconstruction leads to reduction in image noise, which is often equated with an effective increase in system sensitivity. TOF-PET is also not a new idea and was already used in the 1980s [9]. Only the availability of suitable scintillators, fast, low-cost light sensors with high sensitivity, and the development of adapted, integrated electronics with very many synchronized, parallel readout channels could lead TOF-PET into clinically applicable products. Very good time resolution and TOF in image reconstructions may also open improved possibilities for systems with partial ring geometry as required for in-beam PET in proton therapy [77].

High-resolution PET system designs for small animal imaging have tremendously benefitted from the development of PSPMTs, offering excellent identification of the interaction position within arrays of very small crystals (1 to 1.5 mm side length) [78–80]. A number of preclinical systems have been developed based on SiPM readout, not only for simultaneous PET/MR [81].

Future of PET detectors

While sensitivity is increased by larger solid angle coverage, further improvement in image quality can be achieved by TOF-PET including appropriate reconstruction algorithms. The race to ever-improving temporal resolution [82] is not yet over, and the answer to whether the dream of reconstruction-free PET imaging (requiring system time resolution of 10 ps) can become a reality may be 20 years away. Nevertheless, initial, very exciting efforts in this direction are currently underway [83].

Declaration of Competing Interest

The authors declare that they have no known competing financial interests or personal relationships that could have appeared to influence the work reported in this paper.

References

[1] Melcher CL. Scintillation crystals for PET. J Nucl Med 2000;41:1051–1055.
[2] Brownell G, Sweet W. Localization of brain tumors with positron amitters. Nucleonics 1953;11:40–45.
[3] Nestor O, Huang C. Bismuth germanate: a high-Z gamma-ray and charged particle detector. IEEE Trans Nucl Sci 1975;22:68–71.
[4] Cho Z, Farukhi M. Bismuth germanate as a potential scintillation detector in positron cameras. J Nucl Med 1977;18:840–844.
[5] Melcher CL, Schweitzer JS. Cerium-doped lutetium oxyorthosilicate: A fast, efficient new scintillator. IEEE Trans Nucl Sci 1992;39:502–505.
[6] Cooke D, McClellan K, Bennett BL, Roper J, Whittaker MT, Muenchausen RE, et al. Crystal growth and optical characterization of cerium-doped Lu 1.8 Y 0.2 SiO 5. J Appl Phys 2000;88:7360–7362.
[7] Lewellen T, Bice A, Harrison R, Pencke M, Link J. Performance measurements of the SP3000/UW time-of-flight positron emission tomograph. IEEE Trans Nucl Sci 1988;35:665–669.
[8] Mazoyer B, Trebossen R, Schoukroun C, Verrey B, Syrota A, Vacher J, et al. Physical characteristics of TTV03, a new high spatial resolution time-of-flight positron tomograph. IEEE Trans Nucl Sci 1990;37:778–782.
[9] Ter-Pogossian MM, Ficke DC, Yamamoto M, Hood JT. Super PETT I: A Positron Emission Tomograph Utilizing Photon Time-of-Flight Information. IEEE Trans Med Imaging 1982;1:179–187.
[10] Daube-Witherspoon M, Surti S, Perkins A, Kyba C, Wiener R, Werner M, et al. The imaging performance of a LaBr 3-based PET scanner. Phys Med Biol 2009;55:45.
[11] Schaart DR, Schramm G, Nuyts J, Surti S. Time of flight in perspective: instrumental and computational aspects of time resolution in positron emission tomography. IEEE Trans Radiat Plasma Medical Sci 2021;5:598–618.
[12] Humm JL, Rosenfeld A, Del Guerra A. From PET detectors to PET scanners. Eur J Nucl Med Mol Imaging 2003;30:1574–1597.
[13] Becker W. Advanced time-correlated single photon counting techniques. Springer Science & Business Media; 2005.
[14] Hamamatsu Photonics KK, Photomultiplier Tubes, Basics and Applications, Hamamatsu Photonics KK, 2007.
[15] Kyushima H, Shimoi H, Atsumi A, Ito M, Oba K, Yoshizawa Y. The development of flat panel PMT. 2000 IEEE Nuclear Science Symposium. Conference Record (Cat. No. 00CH37149), vol. 1. IEEE; 2000. p. 7/3–7/7.
[16] Shao Y, Silverman RW, Cherry SR. Evaluation of Hamamatsu R5900 series PMTs for readout of high-resolution scintillator arrays. Nucl Instrum Methods Phys Res, Sect A 2000;454:379–388.

[17] Renker D, Lorenz E. Advances in solid state photon detectors. J Instrum 2009;4:P04004.
[18] Jiang W, Chalich Y, Deen MJ. Sensors for positron emission tomography applications. Sensors 2019;19:5019.
[19] Pichler BJ, Bernecker F, Boening G, Rafecas M, Pimpl W, Schwaiger M, et al. A 4x8 APD array, consisting of two monolithic silicon wafers, coupled to a 32-channel LSO matrix for high-resolution PET. IEEE Trans Nucl Sci 2001;48:1391–1396.
[20] McElroy DP, Pimpl W, Pichler BJ, Rafecas M, Schüler T, Ziegler SI. Characterization and Readout of MADPET-II Detector Modules: Validation of a Unique Design Concept for High Resolution Small Animal PET. IEEE Trans Nucl Sci 2005;52:199–204.
[21] Roncali E, Cherry SR. Application of silicon photomultipliers to positron emission tomography. Ann Biomed Eng 2011;39:1358–1377.
[22] Pichler B, Lorenz E, Mirzoyan R, Pimpl W, Roder F, Schwaiger M, et al. Performance test of a LSO-APD PET module in a 9.4 Tesla magnet. IEEE Nuclear Science Symposium and Medical Imaging Conference, Albuquerque, 1997.
[23] Grazioso R, Zhang N, Corbeil J, Schmand M, Ladebeck R, Vester M, et al. APD-based PET detector for simultaneous PET/MR imaging. Nucl Instrum Methods Phys Res, Sect A 2006;569:301–305.
[24] Judenhofer MS, Wehrl HF, Newport DF, Catana C, Siegel SB, Becker M, et al. Simultaneous PET-MRI: a new approach for functional and morphological imaging. Nat Med 2008;14:459–465.
[25] Wu Y, Catana C, Farrell R, Dokhale PA, Shah KS, Qi J, et al. PET performance evaluation of an MR-compatible PET insert. IEEE Trans Nucl Sci 2009;56:574–580.
[26] Delso G, Fürst S, Jakoby B, Ladebeck R, Ganter C, Nekolla SG, et al. Performance measurements of the Siemens mMR integrated whole-body PET/MR scanner. J Nucl Med 2011;52:1914–1922.
[27] Buzhan P, Dolgoshein B, Filatov L, Ilyin A, Kantzerov V, Kaplin V, et al. Silicon photomultiplier and its possible applications. Nucl Instrum and Methods Phys Res Section A: Accelerat, Spectrometers, Detectors Assoc Equip 2003;504:48–52.
[28] Hawkes R, Lucas A, Stevick J, Llosa G, Marcatili S, Piemonte C, et al. Silicon photomultiplier performance tests in magnetic resonance pulsed fields. In: 2007 IEEE Nuclear Science Symposium Conference Record. IEEE; 2007. p. 3400–3403.
[29] Omidvari N, Cabello J, Topping G, Schneider FR, Paul S, Schwaiger M, et al. PET performance evaluation of MADPET4: a small animal PET insert for a 7 T MRI scanner. Phys Med Biol 2017;62:8671.
[30] Levin CS, Maramraju SH, Khalighi MM, Deller TW, Delso G, Jansen F. Design features and mutual compatibility studies of the time-of-flight PET capable GE SIGNA PET/MR system. IEEE Trans Med Imaging 2016;35:1907–1914.
[31] Schaart DR, Seifert S, Vinke R, van Dam HT, Dendooven P, Lohner H, et al. LaBr(3): Ce and SiPMs for time-of-flight PET: achieving 100 ps coincidence resolving time. Phys Med Biol 2010;55:N179–N189.
[32] Spanoudaki VC, Levin CS. Photo-detectors for time of flight positron emission tomography (ToF-PET). Sensors 2010;10:10484–10505.
[33] Solid State Division Hamamatsu Photonics KK, https://www.hamamatsu.com/eu/en/product/optical-sensors/mppc/what_is_mppc.html.
[34] Schaart DR, Charbon E, Frach T, Schulz V. Advances in digital SiPMs and their application in biomedical imaging. Nucl Instrum Methods Phys Res, Sect A 2016;809:31–52.
[35] Rausch I, Ruiz A, Valverde-Pascual I, Cal-González J, Beyer T, Carrio I. Performance evaluation of the Vereos PET/CT system according to the NEMA NU2-2012 standard. J Nucl Med 2019;60:561–567.
[36] Karp JS, Viswanath V, Geagan MJ, Muehllehner G, Pantel AR, Parma MJ, et al. PennPET explorer: design and preliminary performance of a whole-body imager. J Nucl Med 2020;61:136–143.
[37] Gonzalez-Montoro A, Gonzalez AJ, Pourashraf S, Miyaoka RS, Bruyndonckx P, Chinn G, et al. Evolution of PET detectors and event positioning algorithms using monolithic scintillation crystals. IEEE Trans Radiat Plasma Medical Sci 2021;5:282–305.
[38] Casey ME, Nutt R. Multicrystal two dimensional BGO detector system for positron emission tomography. IEEE Trans Nucl Sci 1986;33:460–463.
[39] Ritzer C, Becker R, Buck A, Commichau V, Debus J, Djambazov L, et al. Initial Characterization of the SAFIR Prototype PET-MR Scanner. IEEE Trans Radiat Plasma Medical Sci 2020;4:613–621.
[40] Ota R, Omura T, Yamada R, Miwa T, Watanabe M. Evaluation of a sub-millimeter resolution PET detector with a 1.2 mm pitch TSV-MPPC array one-to-one coupled to LFS scintillator crystals and inter-crystal scatter studies with individual signal readout. IEEE Trans Radiation Plasma Medical Sci 2016;1:15–22.
[41] Anger HO. Scintillation camera. Rev Sci Instrum 1958;29:27–33.
[42] Cherry S, Sorenson J, Phelps M. Block Detectors. Physics in Nuclear Medicine. 3rd ed. Philadelphia, Pa: Elsevier Science (USA); 2003. p. 342–344.
[43] Schmitz RE, Alessio AM, Kinahan PE, Mason NS, Lin EC. The physics of PET/Ct scanners. In: Lin EG, Alavi A, editors. PET and PET/CT: A clinical guide. New York, NY: Thieme; 2005. p. 3–14.
[44] Benlloch J, Carrilero V, González AJ, Catret J, Lerche CW, Abellán D, et al. Scanner calibration of a small animal PET camera based on continuous LSO crystals and flat panel PSPMTs. Nucl Instrum Methods Phys Res, Sect A 2007;571:26–29.
[45] Llosá G, Barrillon P, Barrio J, Bisogni M, Cabello J, Del Guerra A, et al. High performance detector head for PET and PET/MR with continuous crystals and SiPMs. Nucl Instrum Methods Phys Res, Sect A 2013;702:3–5.
[46] Maas MC, Van Der Laan D, Schaart DR, Huizenga J, Brouwer J, Bruyndonckx P, et al. Experimental characterization of monolithic-crystal small animal PET detectors read out by APD arrays. IEEE Trans Nucl Sci 2006;53:1071–1077.
[47] González-Montoro A, Sánchez F, Bruyndonckx P, Cañizares G, Benlloch JM, González AJ. Novel method to measure the intrinsic spatial resolution in PET detectors based on monolithic crystals. Nucl Instrum Methods Phys Res, Sect A 2019;920:58–67.
[48] Stickel JR, Cherry SR. High-resolution PET detector design: modelling components of intrinsic spatial resolution. Phys Med Biol 2004;50:179.
[49] Moehrs S, Del Guerra A, Herbert DJ, Mandelkern MA. A detector head design for small-animal PET with silicon photomultipliers (SiPM). Phys Med Biol 2006;51:1113.
[50] Gonzalez-Montoro A, Pierce LA, Hunter WC, González AJ, Miyaoka RS. Validation of photon collimation techniques for monolithic PET detector calibration. IEEE Trans Radiat Plasma Medical Sci 2020;5:783–792.
[51] Hunter WC, Barrett HH, Lewellen TK, Miyaoka RS. Multiple-hit parameter estimation in monolithic detectors. IEEE Trans Med Imaging 2012;32:329–337.
[52] González-Montoro A, Aguilar A, Cañizares G, Conde P, Hernández L, Vidal LF, et al. Performance study of a large monolithic LYSO PET detector with accurate photon DOI using retroreflector layers. IEEE Trans Radiat Plasma Medical Sci 2017;1:229-237..
[53] Vinke R, Levin CS. A method to achieve spatial linearity and uniform resolution at the edges of monolithic scintillation crystal detectors. Phys Med Biol 2014;59:2975.
[54] Miyaoka RS, Li X, Lockhart C, Lewellen TK. New continuous miniature crystal element (cMiCE) detector geometries. In: 2009 IEEE Nuclear Science Symposium Conference Record (NSS/MIC). IEEE; 2009. p. 3639–3642.

[55] Joung J, Miyaoka RS, Lewellen TK. cMiCE: a high resolution animal PET using continuous LSO with a statistics based positioning scheme. Nucl Instrum Methods Phys Res, Sect A 2002;489:584–598.
[56] Jagoda E, Vaquero J, Seidel J, Green MV, Eckelman WC. Experiment assessment of mass effects in the rat: implications for small animal PET imaging. Nucl Med Biol 2004;31:771–779.
[57] Cherry SR, Dahlbom M. PET: physics, instrumentation, and scanners. PET: Springer; 2006. p. 1–117.
[58] Chang C-M, Cates JW, Levin CS. Time-over-threshold for pulse shape discrimination in a time-of-flight phoswich PET detector. Phys Med Biol 2016;62:258.
[59] Saoudi A, Pepin CM, Dion F, Bentourkia M, Lecomte R, Andreaco M, et al. Investigation of depth-of-interaction by pulse shape discrimination in multicrystal detectors read out by avalanche photodiodes. IEEE Trans Nucl Sci 1999;46:462–467.
[60] Schmall JP, Surti S, Karp JS. Characterization of stacked-crystal PET detector designs for measurement of both TOF and DOI. Phys Med Biol 2015;60:3549.
[61] Thompson CJ, Goertzen AL, Berg EJ, Retière F, Kozlowski P, Ryner L, et al. Evaluation of high density pixellated crystal blocks with SiPM readout as candidates for PET/MR detectors in a small animal PET insert. IEEE Trans Nucl Sci 2012;59:1791–1797.
[62] Nishikido F, Tachibana A, Obata T, Inadama N, Yoshida E, Suga M, et al. Development of 1.45-mm resolution four-layer DOI–PET detector for simultaneous measurement in 3T MRI. Radiol Phys Technol 2015;8:111–119.
[63] González AJ, Majewski S, Sánchez F, Aussenhofer S, Aguilar A, Conde P, et al. The MINDView brain PET detector, feasibility study based on SiPM arrays. Nucl Instrum Methods Phys Res, Sect A 2016;818:82–90.
[64] Inadama N, Hirano Y, Nishikido F, Murayama H, Yamaya T. Development of a DOI PET detector having the structure of the X'tal cube extended in one direction. IEEE Trans Nucl Sci 2016;63:2509-2516.
[65] Li X, Ruiz-Gonzalez M, Furenlid LR. An edge-readout, multilayer detector for positron emission tomography. Med Phys 2018;45:2425–2438.
[66] Peng P, Judenhofer MS, Cherry SR. Compton PET: a layered structure PET detector with high performance. Phys Med Biol 2019;64:10LT01.
[67] Shao Y, Silverman R, Farrell R, Cirignano L, Grazioso R, Shah K, et al. Design studies of a high resolution PET detector using APD arrays. IEEE Trans Nucl Sci 2000;47:1051–1057.
[68] Abreu MC, Aguiar JD, Almeida FG, Almeida P, Bento P, Carriço B, et al. Design and evaluation of the Clear-PEM scanner for positron emission mammography. IEEE Trans Nucl Sci 2006;53:71–77.
[69] Pizzichemi M, Stringhini G, Niknejad T, Liu Z, Lecoq P, Tavernier S, et al. A new method for depth of interaction determination in PET detectors. Phys Med Biol 2016;61:4679.
[70] Zatcepin A, Pizzichemi M, Polesel A, Paganoni M, Auffray E, Ziegler SI, et al. Improving depth-of-interaction resolution in pixellated PET detectors using neural networks. Phys Med Biol 2020;65:175017.
[71] Berg E, Roncali E, Hutchcroft W, Qi J, Cherry SR. Improving depth, energy and timing estimation in PET detectors with deconvolution and maximum likelihood pulse shape discrimination. IEEE Trans Med Imaging 2016;35:2436–2446.
[72] Spencer BA, Berg E, Schmall JP, Omidvari N, Leung EK, Abdelhafez YG, et al. Performance evaluation of the uEXPLORER total-body PET/CT scanner based on NEMA NU 2–2018 with additional tests to characterize PET scanners with a long axial field of view. J Nucl Med 2021;62:861–870.
[73] Ra JB, Lim C, Cho Z, Hilal S, Correll J. A true three-dimensional reconstruction algorithm for the spherical positron emission tomograph. Phys Med Biol 1982;27:37.
[74] Badawi RD, Shi H, Hu P, Chen S, Xu T, Price PM, et al. First human imaging studies with the EXPLORER total-body PET scanner. J Nucl Med 2019;60:299–303.
[75] Vandenberghe S, Moskal P, Karp JS. State of the art in total body PET. EJNMMI Phys 2020;7:1–33.
[76] Van Sluis J, De Jong J, Schaar J, Noordzij W, Van Snick P, Dierckx R, et al. Performance characteristics of the digital biograph vision PET/CT system. J Nucl Med 2019;60:1031–1036.
[77] Surti S, Zou W, Daube-Witherspoon M, McDonough J, Karp J. Design study of an in situ PET scanner for use in proton beam therapy. Phys Med Biol 2011;56:2667.
[78] Bao Q, Newport D, Chen M, Stout DB, Chatziioannou AF. Performance evaluation of the inveon dedicated PET preclinical tomograph based on the NEMA NU-4 standards. J Nucl Med 2009;50:401–408.
[79] Szanda I, Mackewn J, Patay G, Major P, Sunassee K, Mullen GE, et al. National Electrical Manufacturers Association NU-4 performance evaluation of the PET component of the NanoPET/CT preclinical PET/CT scanner. J Nucl Med 2011;52:1741–1747.
[80] Tai Y-C, Chatziioannou AF, Yang Y, Silverman RW, Meadors K, Siegel S, et al. MicroPET II: design, development and initial performance of an improved microPET scanner for small-animal imaging. Phys Med Biol 2003;48:1519–1537.
[81] Miyaoka RS, Lehnert AL. Small animal PET: a review of what we have done and where we are going. Phys Med Biol 2020;65:24TR04.
[82] Lecoq P, Morel C, Prior JO, Visvikis D, Gundacker S, Auffray E, et al. Roadmap toward the 10 ps time-of-flight PET challenge. Phys Med Biol 2020;65:21RM01.
[83] Kwon SI, Ota R, Berg E, Hashimoto F, Nakajima K, Ogawa I, et al. Ultrafast timing enables reconstruction-free positron emission imaging. Nat Photonics 2021;15:914–918.